Multiparametric Tissue Characterization of Brain Neoplasms and Their Recurrence Using Pattern Classification of MR Images[1]

Ragini Verma, PhD, Evangelia I. Zacharaki, PhD, Yangming Ou, Hongmin Cai, Sanjeev Chawla, PhD, Seung-Koo Lee, MD, Elias R. Melhem, PhD, MD, Ronald Wolf, MD, Christos Davatzikos, PhD

Rationale and Objectives. Treatment of brain neoplasms can greatly benefit from better delineation of bulk neoplasm boundary and the extent and degree of more subtle neoplastic infiltration. Magnetic resonance imaging (MRI) is the primary imaging modality for evaluation before and after therapy, typically combining conventional sequences with more advanced techniques such as perfusion-weighted imaging and diffusion tensor imaging (DTI). The purpose of this study is to quantify the multiparametric imaging profile of neoplasms by integrating structural MRI and DTI via statistical image analysis methods to potentially capture complex and subtle tissue characteristics that are not obvious from any individual image or parameter.

Materials and Methods. Five structural MRI sequences, namely, B0, diffusion-weighted images, fluid-attenuated inversion recovery, T1-weighted, and gadolinium-enhanced T1-weighted, and two scalar maps computed from DTI (ie, fractional anisotropy and apparent diffusion coefficient) are used to create an intensity-based tissue profile. This is incorporated into a nonlinear pattern classification technique to create a multiparametric probabilistic tissue characterization, which is applied to data from 14 patients with newly diagnosed primary high-grade neoplasms who have not received any therapy before imaging.

Results. Preliminary results demonstrate that this multiparametric tissue characterization helps to better differentiate among neoplasm, edema, and healthy tissue, and to identify tissue that is likely to progress to neoplasm in the future. This has been validated on expert assessed tissue.

Conclusion. This approach has potential applications in treatment, aiding computer-assisted surgery by determining the spatial distributions of healthy and neoplastic tissue, as well as in identifying tissue that is relatively more prone to tumor recurrence.

Key Words. Brain neoplasm; recurrence; pattern classification; magnetic resonance imaging (MRI); multiparametric MRI; diffusion tensor imaging; computer-aided diagnosis; tumor segmentation.

© AUR, 2008

Treatment of brain neoplasms varies with their type, grade, location, and extent, and often includes a combination of surgical resection and chemoradiation. This can greatly benefit from better delineation of bulk neoplasm boundary, as well as knowledge of the extent and degree of neoplastic infiltration. The true boundary of many neoplasms is difficult to identify with conventional approaches, especially in gliomas that are diffuse and infiltrative. Relatively advanced imaging strategies, such as

Acad Radiol 2008; 15:966–977

[1] From the Department of Radiology, University of Pennsylvania, 3600 Market Street, Suite 380, Philadelphia, PA 19104 (R.V., E.I.Z., Y.O., H.C., S.C., S.-K.L., E.R.M., R.W., C.D.). Received November 20, 2007; accepted January 31, 2008. **Address correspondence to:** E.I.Z. e-mail: Eva.Zacharaki@uphs.upenn.edu

© AUR, 2008
doi:10.1016/j.acra.2008.01.029

perfusion-weighted imaging (PWI), magnetic resonance spectroscopy (MRS), and diffusion tensor imaging (DTI), have improved evaluation in this regard, but remain limited. Tissue characterization is difficult because neoplasms are often heterogeneous, and different histopathologic grades can be present throughout an individual neoplasm. Because the treatment planning of brain neoplasms typically seeks to reduce risk for severe functional loss, large portions of brain neoplasms may remain untreated or suboptimally treated such that time to recurrence shortens and prognosis worsens.

Clinical decisions regarding glioma treatments rely, in part, on magnetic resonance imaging (MRI) before and after surgery as well as follow-up during and after chemoradiation. Routine MRI sequences such as fluid-attenuated inversion recovery (FLAIR) and contrast-enhanced T1-weighted MR images are used to obtain estimates of enhancing and nonenhancing tissue, as well as of edema (ED) or gliosis. However, this process is time and labor intensive, susceptible to inter-rater variability, and often inaccurate, especially in the setting of treatment-related necrosis versus recurrence/progression. Clinical decision making has been aided by the efforts of the medical image analysis community in developing MRI-based automated tumor detection and segmentation (1–9).

A simplified view of a brain neoplasm includes enhancing neoplasm/tumor (ET) tissue and nonenhancing tissue (NET) (solid tissue) and ED (diffuse tissue). Because the manifestation of each of these tissue types varies across subjects and has different underlying pathologic substrates depending on the neoplasm type, there has been growing interest in image-based objective identification of these tissue types as well as possible infiltration. For example, a combination of T1 (with and without intravenous contrast), T2-, and proton density (PD)-weighted images have been used in a fuzzy clustering framework to segment ET (6) and NET (5). FLAIR images show infiltrating neoplasm and ED with relatively high contrast. Nonconventional imaging protocols, such as diffusion-weighted imaging (DWI) and cerebral blood volume (CBV) maps calculated from PWI, have demonstrated the ability to discriminate between high- and low-grade neoplasms and also to study prognosis or predict outcome but are nonspecific in identifying tumor boundary (10–12). DTI (13) has been used for determining fiber tract deformation as a result of neoplasm growth (14–17), as well as to study the progression or infiltration of the neoplasm along white matter tracts (18,19). Some studies have used anisotropy and diffusivity information provided by fractional anisotropy and apparent diffusion coefficient maps computed from DTI data for differentiation of infiltrating neoplasm and ED (14,18–21). DTI metrics have also shown potential in discriminating tumor recurrence from radiation-induced necrosis (22).

A few key issues are apparent with regard to the potential of multiparametric MRI in studying brain tumors. First, although individual MR modalities provide information about some aspects of the tumor, no single modality is capable of providing a comprehensive tissue characterization. Properly combining such diverse MR protocols is likely to enhance discriminatory power and specificity and to better highlight the extent and degree of tumor infiltration. Second, tissue characterization that reveals the degree and extent of infiltration is important for tumor characterization in addition to bulk tumor segmentation; however, little has been done to identify the likelihood of recurrence in the tissue surrounding the neoplasm, based on multiparametric imaging. Third, most of the methods developed have not used advanced pattern classification techniques to discern the patterns of tissue types and infiltration or increase the objectivity of interpretation.

The present work proposes a multiparametric neoplastic tissue characterization that incorporates high-dimensional intensity features created from multiple MRI acquisition protocols (structural MRI as well as DTI) into a pattern classification framework, to obtain a voxel-wise probabilistic spatial map called a “tissue abnormality map” that reflects the likelihood that a given voxel (spatial location) is healthy tissue, tumor, ED, neoplastic infiltration, or a combination thereof. Moreover, by using machine learning methods guided by the follow-up scans, the likelihood of a region presenting tumor recurrence after treatment is determined. By evaluating patients with several different high-grade brain neoplasms and using expert interpretation as a standard, it is demonstrated that such probabilistic tissue characterization is able to better differentiate neoplastic infiltration, ED, and healthy tissue than any single MR modality. More generally, it has been able to produce a subtle characterization of tumor tissue and surrounding tissue and identify regions that later present recurrence. The accuracy of segmentation has been assessed on samples provided by experts. This study is one of the first to investigate integration of multiple MRI parameters via sophisticated nonlinear pattern classification methods to obtain a better characterization of the tumor and the surrounding tissue, as well as to investigate imaging profiles of tissue that are relatively more likely to present tumor recurrence in follow-up scans.

MATERIALS AND METHODS

We propose a multiparametric framework for tissue classification and production of probabilistic maps of tissue abnormality and tumor recurrence. Intensity-based features computed from expert-defined training samples are integrated via a pattern classification technique into a multiparametric imaging profile that aims at classifying brain tissue into each of the following classes: ET, NET, ED, white matter (WM), gray matter (GM), and cerebrospinal fluid (CSF). This multiparametric tissue profile for neoplasms using preoperative imaging can be extended to postoperative follow up scans to determine regions that demonstrate high likelihood of tumor recurrence. This study used an institutional review board–approved protocol that was Health Insurance Portability & Accountability Act compliant. Written informed consent for the routine MR examination was obtained from all patients.

Data Acquisition

We used two datasets, one for creating and validating the tissue abnormality map and the other for generating the recurrence map. In the former, we only have scans of one time point, and in the latter, we have longitudinal scans, across several time points, before and after surgery.

Creation of tissue abnormality map.—The population studied consisted of 14 patients with newly diagnosed primary high-grade brain tumors (eight Grade 3 and seven Grade 4) who had not received any therapy before imaging. The MR data for each patient were acquired either on a 3-T Scanner (Siemens, Trio; Siemens Medical System, Erlangen, Germany) or on a 1.5-T (GE Medical Systems, Genesis Trio; GE, Milwaukee, WI) scanner; the scanner assignment was random (not related to any patient characteristics). The following sequences were acquired: T1-weighted (T1) ($256 \times 192 \times 160$, resolution $0.9765 \times 0.9765 \times 1$, repetition time [TR]: 1,620, echo time [TE]: 3.87), T2 ($512 \times 512 \times 19$, resolution $0.4297 \times 0.4297 \times 6.5$, TR: 4,000, TE: 85), FLAIR ($256 \times 256 \times 46$, resolution $0.9375 \times 0.9375 \times 3$, TR: 1,000, TE: 147), gadolinium-enhanced T1-weighted (GAD) ($256 \times 256 \times 46$, resolution $0.9375 \times 0.9375 \times 3$, TR: 1,000, TE: 147), and DTI ($128 \times 128 \times 40$, resolution: $1.72 \times 1.72 \times 3.0$, 12 gradient directions). Because studies were not always performed on the same scanner because of workflow constraints, there was some variation in measurements (eg, TR, TE). However, special effort was made to make the protocols highly comparable across scanners to avoid introducing confounding variability in the images. For creating the multiparametric tissue profile, we used five structural MR acquisition protocols, namely, DWI, B0, FLAIR, T1, and GAD, and two scalar maps computed from the diffusion tensor images: fractional anisotropy and the apparent diffusion coefficient (13). Figure 1 shows representative slices from each of the acquisition protocols.

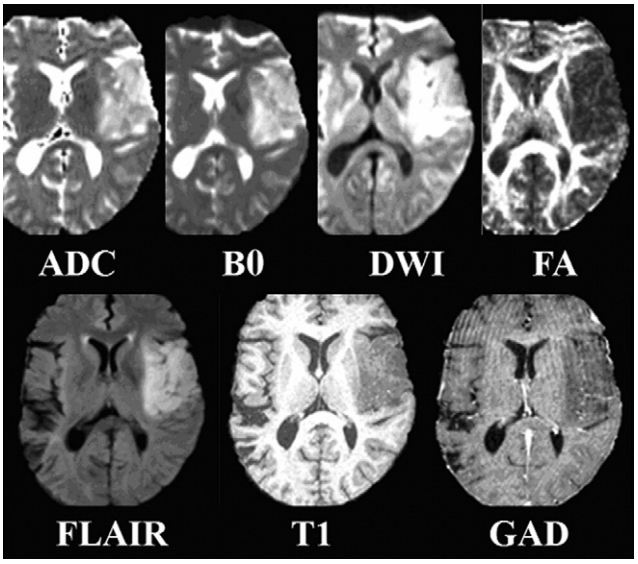

Figure 1. A representative slice from each of the seven co-registered magnetic resonance modalities used in creating the multimodality tissue profile. ADC, apparent diffusion coefficient; B0, baseline (T2-weighted); DWI, diffusion weighted image; FA, fractional anisotropy; FLAIR, fluid attenuated inversion recovery; GAD, gadolinum-enhanced T1-weighted; T1, T1-weighted.

Creation of recurrence maps.—The cases chosen are representative of tumor recurrence as a result of tumor infiltration into surrounding healthy tissue. Our framework focuses on these ambiguous regions that have a mixture of neoplastic and normal tissue characteristics with the aim of classifying them to one of these two classes of normal and neoplastic tissue. The selection of the patients followed three criteria.

1. No evidence for residual enhancing tumor existed after the first resection (based on the clinical reports created by examining the postoperative images acquired within the same day).
2. The patients showed obvious recurrence confirmed by pathology and a second craniotomy.
3. All of the seven MR protocols (required for the multiparametric tissue profile discussed previously) were available in the preresection stage; not all protocols were required in the postresection stage. Specifically, the search in the postresection images for regions with characteristics of recurrence was

mostly based on visual evaluation of FLAIR, T2 and GAD images, and CBV maps (computed from perfusion images). The CBV maps help distinguish between radiation treatment effects and tumor recurrence. None of the images from the postresection scans (including CBV maps) was used in the training for creating the multiparametric profile (probabilistic map).

Of the available brain tumor cases, three cases met all of these criteria and have been included.

Preprocessing

The images are skull stripped and smoothed using the public software package FSL (23). For each of the patients, all the modalities are rigidly co-registered to the T1-weighted image using FSL's registration algorithm, called FLIRT (24) (rigid registration suffices as it is within the same patient). Data are made comparable across patients using histogram matching of intensities. To create the feature vectors, we fuse information from the same voxel across different imaging protocols of the same person. To extend the profile to a recurrence map, we register the follow-up (postresection) images to the preresection image using deformable registration (25), because nonlinear deformations are introduced due to the relaxation of tumor mass effect. The co-registration of all temporal images is important to keep track of changes that reflect tumor progression and for mapping the region of tumor recurrence from the post- to preoperational space.

Design of Tissue Abnormality Feature Vector

We define voxel-wise intensity features using the aligned and preprocessed MRIs. The *intensity feature vector* for each voxel $\vec{x}$ in the three-dimensional image volume I, is defined by concatenating all seven image values:

$$\vec{v}_{\vec{x}} = \left[I_{\vec{x}}^{(ADC)},\ I_{\vec{x}}^{(B0)},\ I_{\vec{x}}^{(DWI)},\ I_{\vec{x}}^{(FA)},\ I_{\vec{x}}^{(FLAIR)},\ I_{\vec{x}}^{(T1)},\ I_{\vec{x}}^{(GAD)} \right]^T$$

where $I_{\vec{x}}^{(M)}$ denotes the intensity of image of modality M at voxel $\vec{x}$. These feature vectors are defined at each voxel in the training samples. To render this feature vector more robust to noise, we incorporate neighborhood information by using four of its neighbors. Seven-dimensional intensity features for these 5 voxels are stacked into a long vector (35-dimensional), which is then used as a feature vector.

Selection of the training samples.—Training samples are identified by an expert neuroradiologist (co-author) by delineating small portions of the tumor tissue types of ET, NET, and ED using the FLAIR and GAD-T1 images. The training samples for ET, NET, and ED are picked very conservatively (only those that have a high certainty according to the expert) as demarcated in red in Fig. 2 (columns 1 and 2). We obtain training samples for the healthy tissue by automatically segmenting the healthy portion of the brain into three classes: WM, GM, and CSF using a k-means segmentation algorithm provided by FSL, called FAST (26), excluding regions close to the tumor. By segmenting the healthy portion of the brain during training, we are able to build a different model for each of the WM, GM, and CSF classes, and therefore avoid the repeated application of a segmentation method, such as FAST, to all new coming brain tumor images. It may be noted that the algorithm is being designed to emulate the knowledge of the expert and hence depends on the expert's definition of the regions. Using multiple experts will increase the size of training samples and is expected to lead to better classifiers. However, conflicting regions of definitions between the experts indicate areas with low certainty about the tissue type. For a more consistent training set, these areas need to be removed from the definition before using them as training samples.

Creation of tissue classifiers and tissue probability maps.—We investigated several pattern classification techniques available in the literature that can help create tissue classifiers. We found that linear multivariate pattern classification techniques such as principal component analysis are easier to apply but they create "global" features for each class that are insufficiently representative for discriminating one tissue class from another, especially when the difference between two classes is very subtle, which is the case in tumor components (NET and ED) and in infiltration. Support vector machines (SVM) (27) were found to optimally classify the data into two or more classes (28,29). We constructed two kinds of classifiers using two different nonlinear classification strategies optimized for the respective application: 1) *intrapatient classifier*: Bayesian classifiers (30) trained using expert defined training samples from within a single patient; and 2) *interpatient classifier*: SVM classifiers trained by combining samples from several patients. For the purpose of comparison, Bayesian classifiers are also constructed using

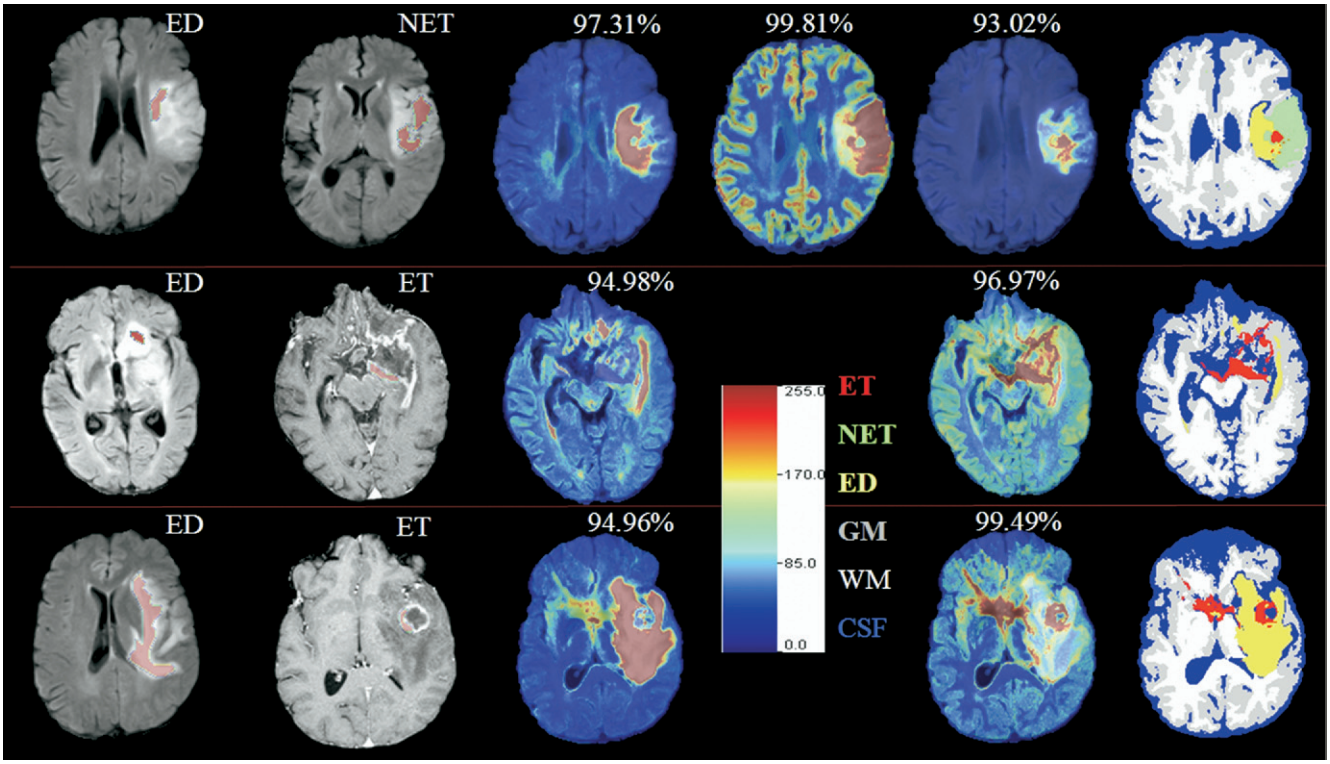

Figure 2. Intrapatient Bayesian classification framework applied to three patients. Each row corresponds to a patient. Columns 1–2 show examples of training samples conservatively chosen by the expert for tissues samples of edema (ED), enhancing neoplasm/tumor (ET), or nonenhancing neoplasm/tumor (NET). Columns 3–5 are the probability maps for ED, NET, and ET, respectively. The numbers in the upper left corners denote the classification rates after segmentation (see column 6). A missing image such as in (2, 4) block indicates the lack of training samples for that tissue class and hence the inability of the classifier to produce the corresponding probability map. The color bar for the probability maps are in block (2, 4). Column 6 shows the segmented image with the color coding of the tissues shown next to the color bar.

data from several patients. Validation of the classifiers is done by creating classifiers using only part of the expert defined training samples, and then applying the classifiers to those excluded samples to determine how well the classification agrees with the expert's interpretation (27). The amount of agreement is referred to as the classification accuracy.

Intrapatient Classification

We use the Bayesian classification method, to design discriminant functions (30) for each of the six tissue classes for a subject, which we refer to as the respective tissue class classifiers. Different discriminant functions designed for each of the six tissue classes (ie, ET, NET, ED, WM, GM, and CSF), evaluated at each voxel, provide the estimate of the probability of that voxel belonging to the respective class, and produce a three-dimensional voxel-wise probability map, called a "tissue abnormality map." There is one tissue abnormality map pertaining to each of the six tissue classifiers produced by assuming multivariate Gaussian distribution for the features. We can obtain tissue segmentation by assigning the voxel to the class having the highest discriminant value among the six classes. This method of tissue classification is optimal when training samples are available for the patient whose tissue needs to be characterized. It effectively replicates the experts' samples to identify regions that are similar. However, only tissue classes (ET, ED, NET) identified by the expert can be characterized for that patient, and because of the conservative nature of sample selection, expert identification may not be provided for all alternate tissue types. This requires pooling samples from several patients and, because of the high variability across individuals, Bayesian classification with its multinomial Gaussian assumption does not provide adequate classification.

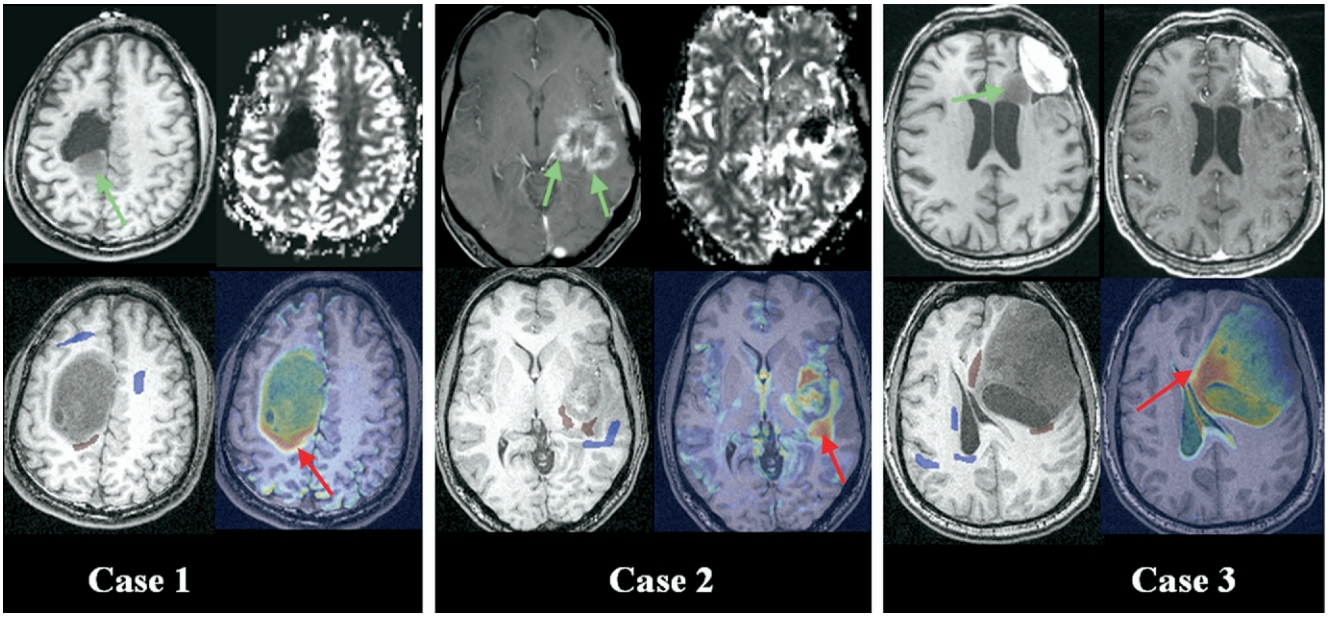

Figure 3. Maps of tumor recurrence for three cases. For each case, the top row shows postresection scans; *green arrows* point to regions identified as suspected of possible recurrence. *Bottom row, left*: Preresection scans showing the regions used for training; *blue* are samples for healthy tissue; *burgundy* are some of the regions identified by an expert as having recurrence in postresection scans when combined with cues obtained from elastic registration. *Bottom row, right*: Probability maps using interpatient classifiers that provide a voxel-wise map of likelihood of tumor recurrence. The color bar is the same as that of Fig. 2 with *red* indicating higher degree of abnormality. *Red arrows* are used to indicate regions in which recurrence actually occurred in follow-up scans.

Interpatient Classification

We combine training samples from across patients, to obtain more generalized tissue classification using SVM. We define six classifiers, one pertaining to each of healthy (WM, GM, and CSF) and neoplasm (ET, NET, and ED) classes (27). Each classifier is created using two sets of training samples: one containing samples of the tissue type for which the classifier is being created and the second class containing samples from all other tissue classes combined together. This is referred to as the one-versus-all framework of creating a classifier and details can be found elsewhere (27). When these classifiers are applied to features defined at voxels in a new brain, they produce a number (SVM classification score) indicative of the class membership (tissue type). This SVM score is then converted to a pseudo-probability score *p_platt* using Platt's method (31). Then the pseudo-*P* values are normalized: $p\_normalized = p\_platt/sum(p)$, where $sum(p\text{-}platt)$ is the sum of pseudo-probabilities for all classes. These voxel-wise pseudo-probability scores form the tissue abnormality map pertaining to that classifier. Responses from the classifiers are combined to obtain tissue segmentation (ie, labels are assigned according to the maximum probability [after normalization]). The classifiers are validated using a similar framework to the one adopted in intrapatient classification.

Design of Recurrence Map

Figure 3 provides examples of recurrence maps for three cases. The top row shows slices from postresection scans: CBV maps computed from perfusion images and T1 images (with/without contrast) that indicate regions of likelihood of recurrence characterized by increased enhancement in GAD (cases 2, 3) and high CBV (case 2) or hypointensity in T1 (cases 1, 3). These are regions indicative of high risk and are pointed out by green arrows. Visual cues gathered from these scans were combined with the cues obtained by elastically registering the postresection scans with the preresection scans (shown in bottom row, left) to account for tissue deformation caused by resection, and to guide the determination of the position of these probable recurrence regions in the preresection scans (marked in burgundy in bottom row). Because no evidence for residual enhancing tumor existed after the resection, these regions were likely to be on or outside the visible tumor boundary in the preresection scans and to have developed an abnormality over time, possibly from tumor infiltration. Samples for the healthy class de-

Table 1
Average (*avg*) Classification Rates and their Standard Deviation (*stdev*) of the Classification Rates, Sensitivity, and Specificity, Over All Subjects for Intrapatient and Interpatient Framework Using Bayesian and SVM Classifications

	Classification Rates						Sensitivity Tumor vs. Healthy	Specificity Tumor vs. Healthy
	ED	ET	NET	CSF	GM	WM		
Bayesian classification (intrapatient)								
Avg	97.03	96.39	93.05	89.68	74.86	82.95	91.84	99.57
Stdev	3.18	3.4	11.82	21.72	6.95	7.73	6.01	0.63
Bayesian classification (interpatient)								
Avg	53.86	86.56	51.11	82.31	66.78	76.06	75.62	94.57
Stdev	47.59	27.74	43.86	15.82	9.22	15.05	36.14	6.12
SVM classification (interpatient)								
Avg	93.38	88.79	34.01	91.34	72.21	85.33	87.54	97.03
Stdev	8.75	29.03	38.71	7.9	12.08	9.45	15.58	3.26

CSF, cerebrospinal fluid; ED, edema; ET, enhancing neoplasm/tumor; GM, gray matter; NET, nonenhancing neoplasm/tumor; SVM, support vector machines; WM, white matter.

picted in blue (Fig. 3, bottom row) were delineated close to the tumor as well as away from it to sample the variability fully. These samples were used to train a two-class SVM classifier. At each instance of training, one patient was left out. Then the classifiers, applied to this left-out patient, produced voxel-wise SVM scores of the tissue at that voxel demonstrating recurrence. These voxel-wise SVM scores comprise a *recurrence probability map* that is indicative of the voxel-wise likelihood of recurrence.

RESULTS

The experiments were conducted with the aim of identifying the applicability of the multiparametric framework in distinguishing between neoplastic tissue types in patients and identifying regions that have a high likelihood of recurrence. In all these experiments, our aim was to produce three-dimensional voxel-wise spatial probability maps for each tumor tissue type; however, we also produced maps of hard segmentation to validate the results visually and empirically. We used classification rates and sensitivity and specificity values, computed on some of the expert-defined samples excluded from training, to provide a measure of degree of certainty in identifying the tumor and the healthy tissue. Classification rate was the percentage of correctly classified voxels with respect to the expert defined samples excluded from training available for that class. Therefore, there was one value for each of the six classes. We took the average over all the subjects for that class to produce the average values for each of the classes.

The sensitivity and specificity are calculated on the two-class problem by grouping together the tumorous tissue types ED, ET, and NET into one class (positive class) and the healthy tissue types CSF, GM, and WM into another class (negative class), respectively. The sensitivity and specificity show the percentage of correctly classified positive and negative samples, respectively. Sensitivity = TP * 100/(TP + FN) and Specificity = TN * 100/(FP + TN), where TP, TN, FN, and FP stand for true positive, true negative, false negative, and false positive, respectively.

Intrapatient Tissue Classification

Figure 2 shows the results of applying the Bayesian classification framework (see Creation of Tissue Classifiers and Tissue Probability Maps) on 3 of the 14 patients. Each row corresponds to a different patient and shows examples of expert-defined neoplastic regions that are used as training samples, the tissue probability maps, as well as hard tissue segmentation obtained from these probability maps. The top left corner of each probability map gives the classification accuracy for that tissue in that patient. For some patients, where the expert was unable to define certain tissue types, such as NET in rows 2 and 3 of Fig. 2, no probability maps could be created. The average classification rates over all datasets can be found in row 1 of Table 1.

Interpatient Tissue Classification

The comparative results of applying the interpatient, Bayesian, and SVM tissue classifiers can be found in Table 1, rows 2 and 3, respectively. As can be observed, Bayesian classification (row 2) performed poorly in the

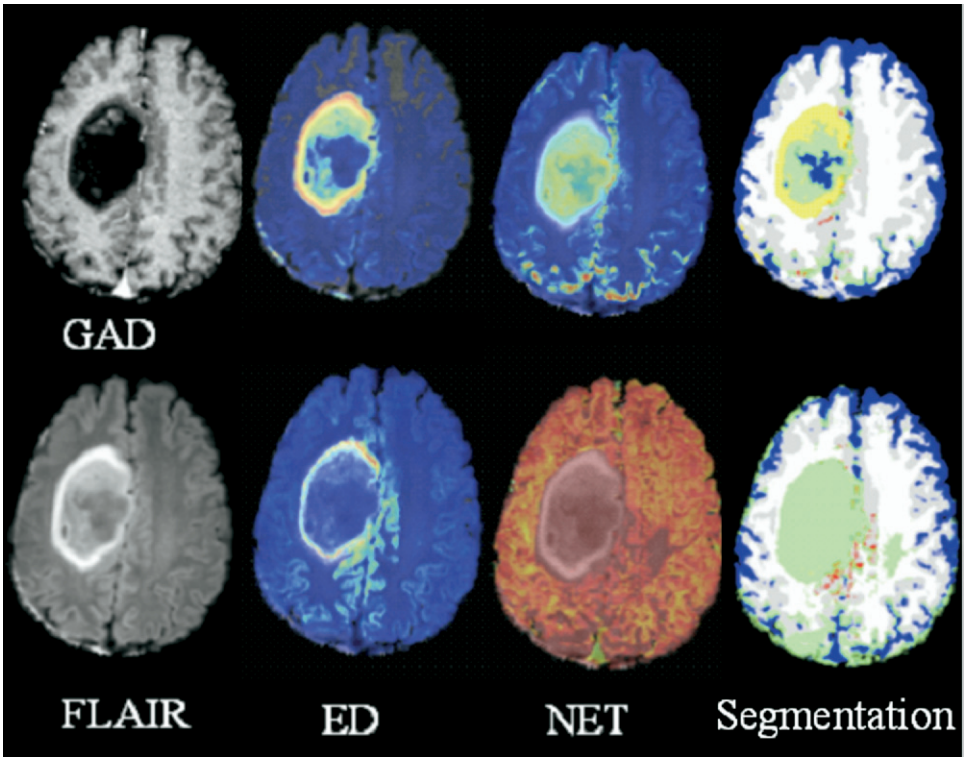

Figure 4. Application of SVM classification (*top row*) and Bayesian classification (*bottom row*) of the neoplasm represented in column 1 by training across patients. Although support vector machines (SVM) classifiers combining information from several patients are able to identify both edema (ED) and nonenhancing neoplasm/tumor (NET), like the expert, the Bayesian classifiers created from this patient alone identify the whole neoplastic region as NET (unlike the expert). The color coding is same as that of Fig. 2. FLAIR, fluid attenuated inversion recovery; GAD, gadolinium-enhanced T1-weighted.

interpatient framework (ie, in the case of increased variability in the data) because of the combination of training samples from several patients compared to the intrapatient Bayesian classification (row 1). By combining the training samples from different patients, we can combine information from patients within a grade and apply it to other patients of the same grade. Empirically, we found that keeping within the grade produces probability maps that are high in specificity. The average sensitivity and specificity for all patients can be found in the last columns of Table 1.

For visual assessment, we show the application of the interpatient tissue classifiers on a case with nonenhancing tumor (Fig. 4) and on a case with enhancing tumor (Fig. 5). The first column in both figures provides slices from the FLAIR and GAD images to indicate the extent and composition of the tumor. The top row 1 (columns 2–4 in Fig. 4 and columns 3–6 in Fig. 5) shows the probability maps and tissue segmentation map obtained by applying the SVM classifiers (see Creation of Tissue Classifiers and Tissue Probability Maps) to this patient and the bottom row presents the Bayesian classifier (created using training samples from all patients except this patient). The comparative classification rates and sensitivity and specificity for these patients are given in Table 2. In Figure 4, there was no ET detected in the tumor; the NET was oversegmented by the Bayesian framework (as is also evident from the tissue probability maps for NET, which shows high false positives). The entire tumor was classified as NET failing to detect the tissue differences. The SVM framework was able to characterize the tumor as a combination of ED and NET and the dark core was classified as CSF, perhaps because of the nature of the tissue. In Figure 5, we see the example of a case in which the Bayesian framework provides better segmentation, which is also reflected in the classification accuracy in Table 2. However, SVM performs better in determining healthy tissue with low false positives.

Analyzing Patterns of Tumor Recurrence

As explained in Design of Recurrence Map, recurrence classifiers created from two patients was then

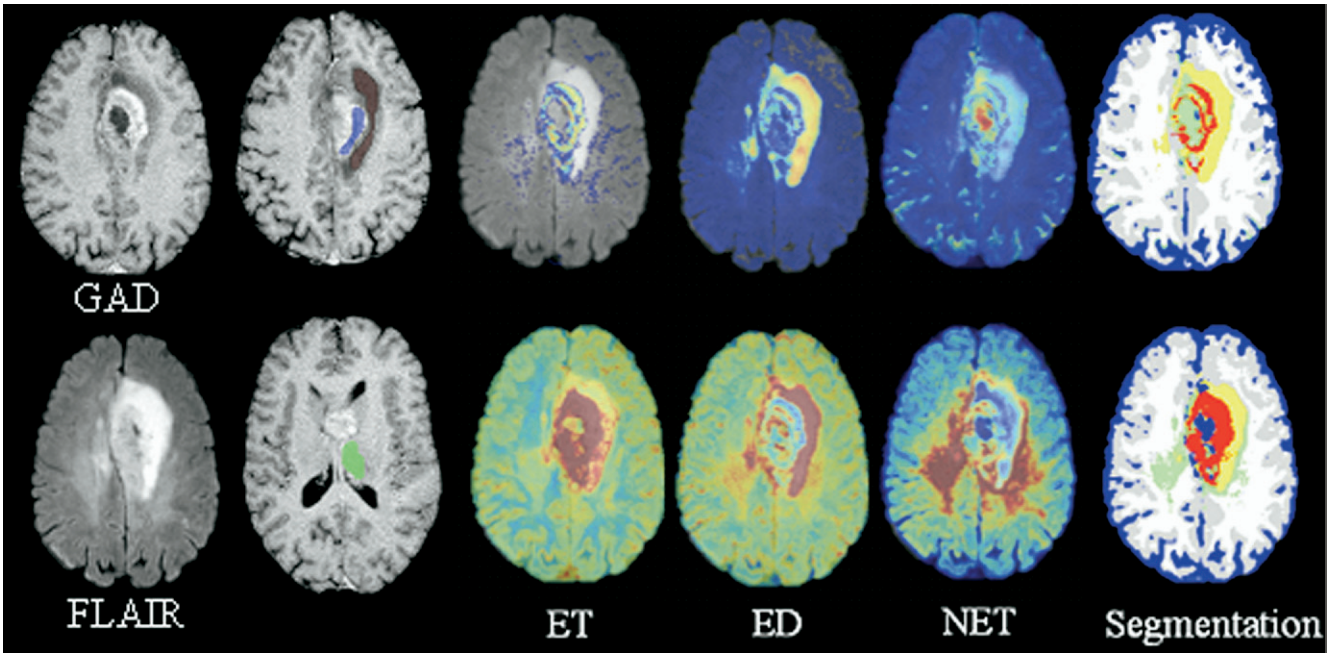

Figure 5. Application of support vector machines (SVM) classification (*top row*) and Bayesian classification (*bottom row*) of the neoplasm represented in column 1 by training across patients using training samples shown in column 2. The SVM classification (*top row, columns 3–6*) is more conservative than the Bayesian classification (*bottom row, columns 3–6*) and better matches the expert. The probability maps using the Bayesian classification seem to identify the edema (ED) well, oversegment the enhancing neoplasm/tumor (ET), and confuse the nonenhancing neoplasm/tumor (NET) with cerebrospinal fluid (CSF). The SVM classification is able to capture the presence of NET (*green*) in the segmented image on top row, along with ED and ET. The color coding is same as that of Fig. 2. FLAIR, fluid attenuated inversion recovery; GAD, gadolinium-enhanced T1-weighted.

applied to the features computed from the preresection scans of the third patient, to create a recurrence probability map, indicative of regions with high likelihood of recurrence. Figure 3, bottom row, right, shows the recurrence probability maps for three cases. Although these results are preliminary and the number of patients is very small to be able to draw a conclusion, it can be observed that regions that were identified as recurrence in these patients, actually showed high probability (red) of abnormality in the preresection scans.

DISCUSSION

In this study, we have created a multiparametric profile for brain tumors, aiming at a comprehensive tissue characterization. Both classification approaches (intra- and interpatient with Bayesian and SVM classification) have the same underlying framework, namely combining conventional structural MRI with DTI, to train classifiers for the tumor types of enhancing and nonenhancing tumor, ED, and healthy tissue. The distinction of the neoplastic tissue from healthy tissue, as well as the identification of different tumor components and ED, as can be seen in Figures 4 and 5, indicates that this multiparametric framework effectively integrates multiprotocol information into a comprehensive tissue profile that can systematically evaluate the extent and heterogeneous composition of the tumor, and accurately replicate the expert's outlining of these regions. Thus, knowing the probable extent of abnormality of the neoplasm in terms of enhancing or nonenhancing tumor type or ED will help better target the treatment of these regions. Existing computerized methods for diagnosis suffer from the absence of validation because of the lack of ground truth. Conventionally, histopathologic examination following a biopsy has been the accepted ground truth. However, its outcome depends on the region sampled and, given the heterogeneity of the tumor, may wrongly indicate the grade of the tumor and the subsequent treatment. The probability measures of our framework are defined on each voxel and therefore capture heterogeneous patterns of tissue pathology. Moreover, these maps may provide sufficient premise to histologically test regions with higher probability of neoplastic content. This would aid in making clinical decisions.

Table 2
Classification Rates Sensitivity and Specificity of Applying the SVM and Bayesian Interpatient Classification Framework to the Two Patients Shown in Figures 4 and 5

Patient in Figure	Classification Rates						Sensitivity Tumor vs. Healthy	Specificity Tumor vs. Healthy
	ED	ET	NET	CSF	GM	WM		
Fig. 4								
SVM	79.78	NA	56.61	78.11	81.99	84.36	71.07	99.49
Bayes	2.28	NA	100	37.01	56.25	60.58	99.98	77.6
Fig. 5								
SVM	100	11.56	NA	99.9	54.66	96.16	81.59	99.97
Bayes	100	99.03	NA	97.87	72.84	61.26	99.02	98.11

CSF, cerebrospinal fluid; ED, edema; ET, enhancing neoplasm/tumor; GM, gray matter; NET, nonenhancing neoplasm/tumor; SVM, support vector machines; WM, white matter.

Overall, the SVM classification performs better than the Bayesian. The low classification rates of healthy tissue are due to these samples being selected through an automated segmentation method, which may have led to errors in training.

Tissue that shows mixture of healthy and neoplastic tissue, with or without ED, may be a precursor to the development of a neoplasm in the future. This is precisely the aim of the experiments that we have conducted on cases that have demonstrated recurrence (Fig. 3). By identifying regions in the preresection scan that correspond to the areas of recurrence in the follow-up scans, we have characterized the imaging profile of abnormal tissue that transformed to a neoplasm. Although we used a small dataset for the identification of regions of high abnormality and high tumor recurrence probability, the quantification of the degree of abnormality by the probability maps in this manner illustrates the concept of anticipating sites of recurrence requiring more aggressive or alternate therapies. Thus, although we may not have always accurately determined the regions of recurrence, we have been able to demonstrate that the regions we predicted to recur, based on the probabilistic maps produced by the classification framework, did actually progress to recurrence.

We have proposed intra- and interpatient approaches to the characterization of neoplastic tissue, based on very conservative training samples identified by experts. The approach that is to be finally adopted depends on the application. If the aim is to replicate the understanding of the expert for a particular patient, as may be the case in a surgery-related decision, then the intrapatient Bayesian framework is appropriate (as can be seen in the classification rates and the overall good segmentation maps in Fig. 2). Although useful for individual patient analysis, such a profile can only be applied to future scans of that patient alone, due to the fact that the profile will not be able to capture the variability across patients. An analysis of the probability and the segmentation maps reveals that the framework might oversegment tissue types such as ET in patient of row 3. Additionally, the intrapatient Bayesian framework is unsuitable for determining a tissue type that the expert is unable to identify, or even do the characterization of the patient for which no training samples are available. This is especially the case when there is a large mass of NET and ED, which is difficult to distinguish even by the expert. When treatment decisions need to be made about surrounding nonenhancing tissue, it is important to have a tissue characterization that will highlight the regions of abnormality. This was the motivation to develop the interpatient framework.

The evaluation of the SVM and Bayesian classification methods in combining tissue samples across patients indicates that SVM performs better. A comparison of rows 2 and 3 of Table 1 shows that the Bayesian classifier has lower sensitivity than the SVM, and also demonstrates increased classification accuracy (with lower variability) for the SVM classifier in all tissue types except NET. Edema identification shows marked improvement. Enhancing neoplasm/tumor is also identified with high classification accuracy based on the expert defined samples. The comparison reveals that NET was the most difficult tissue type to characterize both by the computerized algorithm as well as the experts, demonstrated by the fact that the expert identified the least training samples for NET. This is indicative of the variability in these regions across patients. There is a decrease in the average classification rate of NET from the interpatient Bayesian to the SVM classification, although both are low, which could be due to the low number of training samples to which SVM is sensitive. Based on the improved performance in the other tissue classes, we expect SVM to do better when

we add training samples in the future. Although it may seem that the intrapatient Bayesian classification performs very well in the case of NET, it should be noted that this is only true for patients in whom NET has already been identified by an expert and the average classification rates have been computed only on these few subjects. Analysis of the NET classification results with interpatient classification reveals that it is mostly misclassified as ED, GM, and CSF or a possible combination of these. This could be explained by the fact that NET could have healthy tissue combined with neoplasm and ED, and NET could also be easily misclassified by an expert as well. The superiority of interpatient classification reveals that a combination of information from several patients is crucial for generalizability when a new patient is to be tested in this framework. We propose to use additional features and better SVM based classifiers to pursue interpatient classification of tumor types.

CONCLUSIONS

In summary, we have tested a multiparametric framework for neoplastic tissue characterization using multiple MR acquisition protocols. This abnormality profile helps distinguishing among neoplastic components, ED, and normal tissue, and creating a probabilistic map that indicates the likelihood of tumor recurrence. We expect that our tissue classification will be able to 1) provide a better understanding of the spatial distribution of cancer, thereby assisting in treatment planning either via resection or focused radiotherapy and radiosurgery; 2) potentially enhance the physician's ability to diagnose and segment the tumor; and 3) help identify tissue that can convert to tumor in follow-up cases after resection. The method can thus potentially be used to study tissue changes introduced as a result of radiotherapy, chemotherapy, and medication. Future studies are necessary to provide a more extensive training basis for the classifiers and to further validate the performance of this computer analysis methodology. We also propose to use feature selection schemes to determine the contribution of each of the modalities, so that the modalities best for tissue characterization can be identified and the acquisition protocol streamlined.

REFERENCES

1. Prastawa M, Bullitt E, Ho S, et al. A brain tumor segmentation framework based on outlier detection. Med Image Anal 2004; 8:275–283.
2. Schmidt M, Levner I, Greiner R, et al. Segmenting brain tumors using alignment-based features. The Fourth International Conference on Machine Learning and Applications, Los Angeles, CA, December 2005.
3. Kaus MR, Warfield SK, Nabavi A, et al. Automated segmentation of MR images of brain tumors. Radiology 2001; 218:586–591.
4. Just M, Thelen M. Tissue characterization with T1, T2 and proton density values: results in 160 patients with brain tumors. Radiology 1988; 169:779–785.
5. Fletcher-Heath LM, Hall LO, Goldgof DB, et al. Automatic segmentation of non-enhancing brain tumors in magnetic resonance images. Artif Intell Med 2001; 21:43–63.
6. Clark M, Hall L, Goldgof D, et al. Automatic tumor segmentation using knowledge-based techniques. IEEE Trans Med Imaging 1998; 17:187–201.
7. Young RJ, Knopp EA. Brain MRI: tumor evaluation. J Magn Res Imaging 2006; 24:709–724.
8. Bordignon KC, Neto MC, Ramina R, et al. Patterns of neuroaxis dissemination of gliomas: suggestion of a classification based on magnetic resonance imaging findings. Surg Neurol 2006; 65:472–477.
9. Talos I-F, Zou KH, Ohno-Machado L, et al. Supratentorial low grade glioma resectability: statistical predictive analysis based on anatomic MR features and tumor characteristics. Radiology 2006; 239:506–513.
10. Aronen HJ, Gazit IE, Louis DN, et al. Cerebral blood volume maps of gliomas: comparison with tumor grade and histological findings. Radiology 1994; 191:41–51.
11. Krabbe K, Gideon P, Wagn P, et al. MR diffusion imaging of human intracranial tumors. Neuroradiology 1997; 39:483–489.
12. Provenzale JM, Mukundan S, Baroriak DP. Diffusion-weighted and perfusion MR imaging for brain tumor characterization and assessment of treatment. Radiology 2006; 239:632–649.
13. Bihan DL, Mangin J-F, Poupon C, et al. Diffusion tensor imaging: concepts and applications. J Magnet Reson Imaging 2001; 13:534–546.
14. Nimsky C, Ganslandt O, Hastreiter P, et al. Intraoperative diffusion tensor MR imaging: shifting of white matter tracts during neuro-surgical procedures—initial experience. Radiology 2005; 234:218–225.
15. Field AS, Alexander AL. Diffusion tensor imaging in cerebral tumor diagnosis and therapy. Top Magnet Reson Imaging 2004; 15:315–324.
16. Stieltjes B, Schluter M, Didinger B, et al. Diffusion tensor imaging in primary brain tumors: reproducible quantitative analysis of corpus callosum infiltration and contralateral involvement using a probabilistic mixture model. Neuroimage 2006; 31:531–542.
17. Stadlbauer A, Nimsky C, Buslei R, et al. Diffusion tensor imaging and optimized fiber tracking in glioma patients: histopathologic evaluation of tumor-invaded white matter structures. Neuroimage 2007; 34:949–956.
18. Tummala RP, Chu RM, Liu H, et al. Application of diffusion tensor imaging to magnetic-resonance-guided brain tumor resection. Pediatr Neurosurg 2003; 39:39–43.
19. Mori S, Fredericksen K, Zijl PCM, et al. Brain white matter anatomy of tumor patients evaluated with diffusion tensor imaging. Ann Neurol 2002; 51:377–380.
20. Jellison BJ, Field AS, Medow J, et al. Diffusion tensor imaging of cerebral white matter: a pictorial review of physics, fiber tract anatomy, and tumor imaging patterns. Am J Neuroradiol 2004; 25:356–369.
21. Sundgren PC, Fan X, Weybright P, et al. Differentiation of recurrent brain tumor versus radiation injury using diffusion tensor imaging in patients with new contrast-enhancing lesions. Magnet Reson Imaging 2006; 24:1131–1142.
22. Hein PA, Eskey CJ, Dunn JF, et al. Diffusion-weighted imaging in the follow-up of treated high-grade gliomas: tumor recurrence versus radiation injury. AJNR Am J Neuroradiol 2004; 25:201–209.
23. Smith SM, Jenkinson M, Woolrich MW, et al. Advances in functional and structural MR image analysis and implementation as FSL. Neuroimage 2004; 23:208–219.
24. Jenkinson M, Smith S. A global optimisation method for robust affine registration of brain images. Med Image Anal 2001; 5:143–156.
25. Zacharaki EI, Shen D, Mohamed A, et al. Registration of brain images with tumors: towards the construction of statistical atlases for therapy planning. Arlington, VA: ISBI, 2006.

26. Zhang Y, Brady M, Smith S. Segmentation of brain MR images through a hidden Markov random field model and the expectation maximization algorithm. IEEE Trans Med Imaging 2001; 20:45–57.
27. Schölkopf B, Smola AJ. Learning with kernels: support vector machines, regularization, optimization and beyond (adaptive computation and machine learning). Cambridge, MA: The MIT Press; 2001.
28. LaConte S, Strother S, Cherkassky V, et al. Support vector machines for temporal classification of block design fMRI data. NeuroImage 2005; 26:317–329.
29. Davatzikos C, Shen DG, Wu X, et al. Whole-brain morphometric study of schizophrenia reveals a spatially complex set of focal abnormalities. JAMA Arch Gen Psychiatry 2005; 62:1218–1227.
30. McLachlan GJ. Discriminant analysis and statistical pattern recognition. New York: Wiley-Interscience, 2004 (Wiley Series in Probability and Statistics).
31. Platt J. Probabilistic outputs for support vector machines and comparison to regularized likelihood methods. In: Smola AJ, Bartlett P, Schölkop B, Schuúrmans D, eds. Advances in large margin classifiers. Cambridge, MA: MIT Press, 2000.61–74.